



Symmetrical electrode of active carbon powder for capacitive deionization — surface-modified aluminum plate as current collector

Jiangtao Fu^a, Li Wang^{a,*}, Ning Hu^a, Ze Wang^a, Wei Wang^b

^aSchool of Resources and Environmental Engineering, Wuhan University of Science and Technology, Wuhan 430081, China, email: wanglijohn@hotmail.com (L. Wang)

^bDOW Water & Process Solutions, Shanghai 201203, China

Received 7 August 2017; Accepted 30 January 2018

ABSTRACT

Pure aluminum (Al) plate modified by sodium hydroxide solution and electrochemical methods was used as the current collector for electrodes in capacitive deionization (CDI) process for desalination of NaCl solution. The experimental results show that the modification can greatly improve salt removal from the solution. Compared with the native Al plate and Ni foil current collector CDI electrodes, the modified Al plate CDI achieved a desalination capacity as high as 10.74 mg/g in 400 $\mu\text{s}/\text{cm}$ of NaCl solution. The modification has greatly improved the contact of the current collector and the active material on the interface, leading to a decrease of interfacial and intrinsic resistance in CDI cell and enhancement of the electrical double layer capacitors (EDLCs) of the electrodes, which might be attributed to the improvement of the desalination.

Keywords: CDI; Al plate; Surface modification; Desalination

1. Introduction

Capacitive deionization (CDI) is an electrochemically controlled method for desalination. Anions and cations from aqueous solutions are adsorbed in the electrical double layer region at an electrode–solution interface when an electric potential is applied [1]. When electrodes are saturated with ions, different regeneration modes may be employed, such as electrodes shortening, potential off, or electrodes reversing [2–4]. As a water treatment method, it is environment friendly, energy saving, promising high water recovery, and easy operation [5].

The components of conventional CDI cell including current collectors, electrode-active material, gaskets, spacer, water distribution channels, etc. [6,7]. Researches on CDI were focused on the electrode-active material in recent years [1,8]. However, few researches were conducted on current collector, which is one of the core components of CDI. The function of the current collector is to transfer electrons and

current from DC power to the active material and to serve as supporter for the active material. To enhance operation efficiency, a low interfacial resistance is required to avoid a large voltage drop from the electrode to the current collector [8]. In other words, the active material should firmly adhered with the current collector to reduce the interfacial resistance and enlarge the electrical double layer capacitors (EDLCs). The capacitance of CDI can be represented by to the following equation:

$$C = \frac{I}{m \times dV / dt} \quad (1)$$

where C is the capacitance, I is the constant discharge current in ampere (A), m is the mass of the active material, and dV/dt is the slope in potential per second (V/s). Higher interfacial resistance caused the larger slope of potential leading to a decrease in capacitance. Besides, lower intrinsic resistance of the current collector will reduce the potential drop of electrode and enlarge the capacitance. Furthermore, because

* Corresponding author.

water flushed the surface of electrodes, lower adhesion between the active material and the current collector limits the lifetime of CDI, and it is important to improve the active material/current collector interface contact behavior to reinforce the CDI performance.

The widely used current collector materials include graphite [9–18], titanium (Ti) plate [19–21], stainless steel (SS) plate [22,23], nickel (Ni) plate (foil) [24,25], copper [26], and others [27,28], with their electrical conductivity and excellent formability. However, few words were depicted on the interfacial resistance and contact behavior of the active material/current collector, as well as the influence of intrinsic resistance of these current collector materials on CDI in these researches. These researches actually illustrated the overall properties of CDI electrode, instead of partial on the electrode's active material. The desalination results are naturally biased and deficient.

Aluminum (Al) is widely used as the current collector in lithium-ion batteries [29,30], capacitors, and super capacitors [31,32] because of its low cost, electrical conductivity, density, malleability, and formability. The electrical conductivity and intrinsic resistance of Al is much better than those of graphite, Ti, SS, and Ni. The corrosion stability of Al in typical electrolytes of lithium-ion batteries has been proven by many researchers [30,33]. However, no research has investigated the use of Al as current collector on CDI. In this work, pure Al plate current collectors for CDI electrodes were modified with alkaline and electrochemical etching process, and active carbon (AC) powder was used as the active material to fabricate CDI electrodes. The objective was to cover the pore surface of electrochemically etched Al plate to increase the surface contact at the Al/active material interface, to improve the contact behavior, to reduce the interfacial resistance and intrinsic resistance of the EDLCs, and to obtain an understanding of the mechanism of modified Al plate as the current collector. Comparative studies were conducted on desalination performance and electrochemical properties of different CDI electrodes with modified pure Al plate (M-Al-CDI), Ni foil (Ni-CDI), and native Al plate (N-Al-CDI) as the current collectors.

2. Materials and methods

2.1. Materials

The high purity commercial Al plate used in this research was bought from Guocai Keji (China). Analytical pure chemicals for Al plate pretreatment and etching, and ingredients of the active materials and sodium chloride (NaCl) for the preparation of electrolytic solution were from Zhiyuan Chemical Reagent Co. Ltd. (Tianjin, China). Polyvinylidene fluoride (PVDF) as the binder for electrode preparation was from Solvay (Solef 1015, Belgium).

2.2. Pretreatment and etching process of Al plate

The native pure Al plates were first cut to the designed shape (65 mm * 65 mm * 0.6 mm with 0.5 mm * 3.5 mm piece as electrode terminal, weighting 5.8 g) with scissors. The edges of the specimens were polished to be free of burr by sand papers (400 and 1,000 in mesh). The specimens were then treated by acetone degreasing, followed by etching with

5% NaOH solution at 60°C for 2 min and desmutting in 20% HNO₃ solution for 2 min. The electrochemical etching was conducted to form micropores on the surface (Al plates as the anode and lead as the cathode) in 50°C 10% HCl solutions for 60 s with the current density of 1.5 A/dm². After each step was completed, the specimens were completely rinsed in deionization water to prevent a carryover of the chemicals into the next step.

2.3. Fabrication of electrodes

PVDF solution was prepared by 5 g of PVDF, 35 mL of *N*-dimethylacetamide (DMAC), and 5 mL of polyethylene glycol (PEG-600), and the solution was placed into an ultrasonic dissolving machine for 4 h at 60°C. PEG-600 was used as hydrophilic material because of the hydroxyl in molecule [34]. Then 1 g of graphite powder (325 in mesh) and 20 g of AC powder (325 in mesh, modified by KOH solution [15,35,36]) were added into the solution at 60°C and stirred into slurry with glass rod.

The active material slurry was evenly casted on both sides of the modified Al plate with a blade to form a symmetrical electrode, dried in a vacuum oven at 80°C for 4 h to remove DMAC residual on the electrode, pressed on the bead machine, dried in the vacuum oven at 150°C for 2 h, and cooled in the room temperature. The mass of the active material weight density was 12 mg/cm².

2.4. Desalination experiments setup

Capacitive desalination experiments were conducted in a continuously circulated mode at room temperature, and the schematic diagram was given in Fig. 1. It consisted of a CDI cell, a peristaltic pump (6–50 mL/min, G02A, Runze, Nanjing, China), a conductivity meter (TM-03, Leici, Shanghai, China), and a DC power (IT6724C, ITECH ELECTRONICS, Nanjing, China). The CDI cell consisted of a pair of symmetrical AC powder electrodes, and the gap between electrodes was 1.9 mm. The CDI cell had a good expansibility because the electrodes could be expanded to the required numbers according to the ionic concentration of feed water and requirements of effluents. The effective volume of the CDI cell was 40 mL. The brine water (100 mL NaCl solutions with conductivities of 100, 200, 300, and 400 μS/cm) was continuously pumped into the CDI cell by peristaltic pump with a flow rate of 6 mL/min at the voltage of 1.4 VDC at room temperature, the feed pressure is 20 kPa. The production water conductivity was measured every 2 min by conductivity meter. Desorption experiments were conducted with a flow rate of 50 mL/min. The desalination capacity Q (mg/g AC) could be calculated according to the following equation:

$$Q = \frac{(C_0 - C) \times V_{\text{NaCl}}}{m} \quad (2)$$

where C_0 and C (mg/L) represent the influent and treated stream total dissolved solids, respectively, V_{NaCl} (ml) is the volume of NaCl solution, and m (g) is the mass of AC. The desalination ability of three CDI electrodes with different current collectors was compared at the same operation parameters.

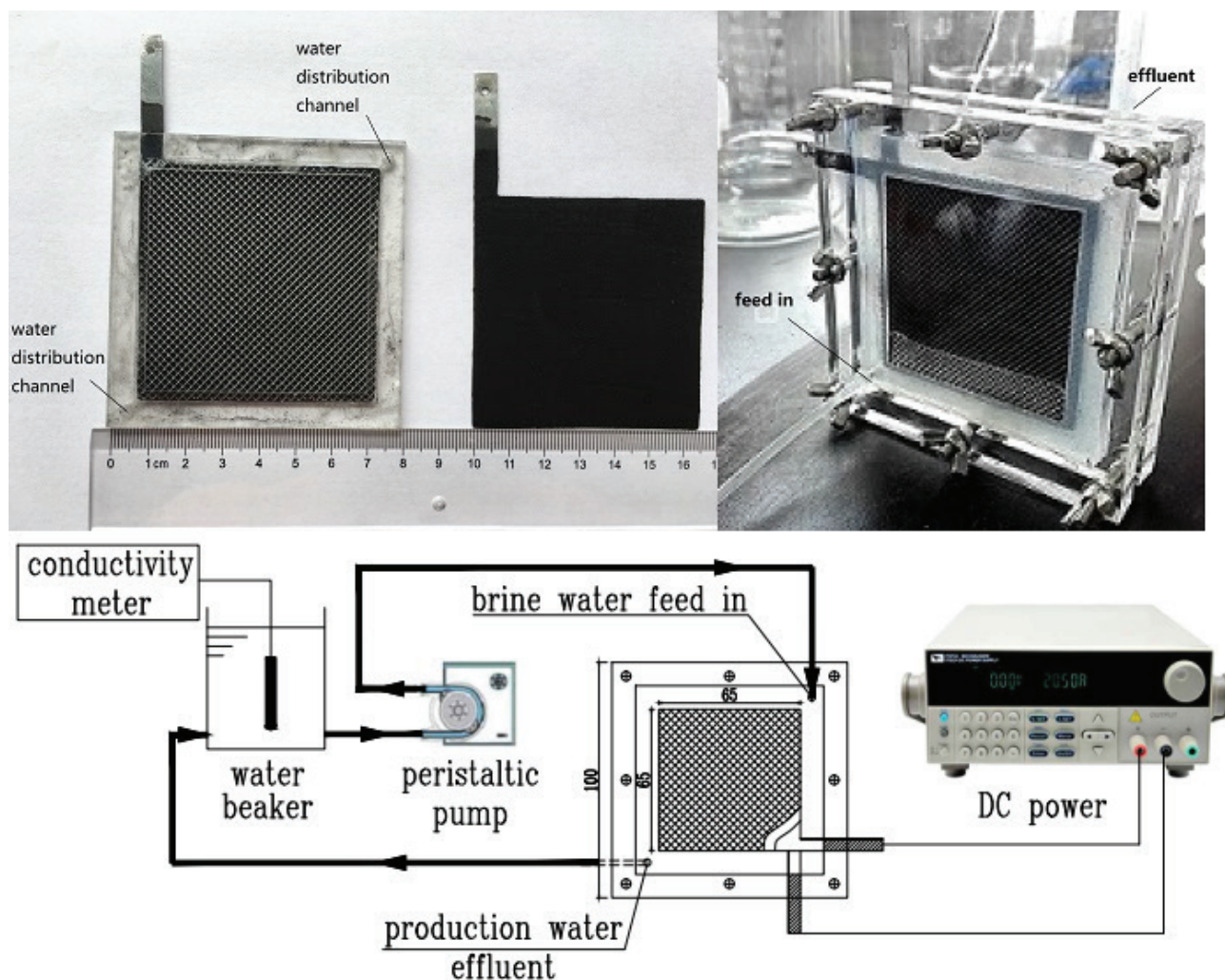


Fig. 1. Schematic diagram of the electrosorption and desorption of CDI.

2.5. Measurements

The morphology and microstructure of the NaOH, electrochemically etched Al plate, and active material were examined using scanning electron microscope (SEM, JSM-6610, JEOL, Japan). The electrochemical behaviors of AC CDI electrodes were monitored using cyclic voltammetry (CV) and electrochemical impedance spectroscopy (EIS) parameter analysis on electrochemical workstation (CHI660E, CH Instruments, China). A three-electrode cell assembly was utilized with an Hg/Hg₂Cl₂ reference electrode, a counter electrode of platinum, and a working electrode (1 × 1 cm²) in a diameter of 100 mL beaker of electrolyte solution. Charge/discharge performance of different CDI electrodes was measured with constant current and flow rate in LAND-CT2001A battery test system.

3. Results and discussion

3.1. Structure and physical behaviors of native Al plate, surface-modified Al plate and active material

Fig. 2 shows the morphologies of native Al plate, NaOH-etched Al plate, electrochemically etched Al plate, and active

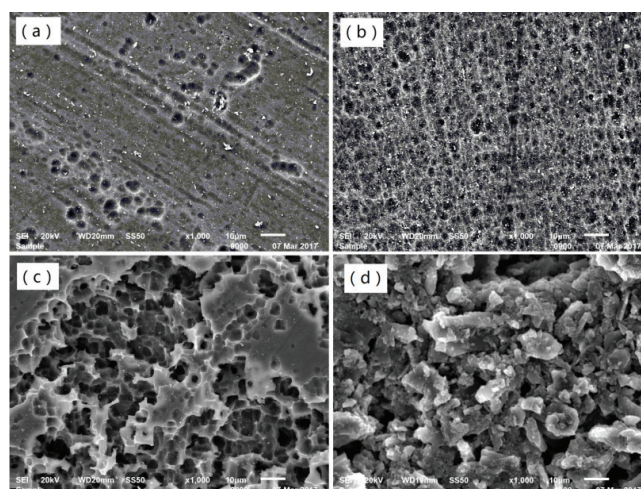


Fig. 2. SEM images of (a) pure Al plate, (b) NaOH etched Al plate, (c) electrochemical etched Al plate, and (d) active material surface.

material surface of electrodes. It can be seen that pure Al plate surface was smooth with few small pores on it. After alkali etching, the surface has turned into rough (Fig. 2(b)). It became a three-dimensional structure with larger pore (Fig. 2(c)), after electrochemical etching. It provided a good primer for the active material to adhere with. Fig. 2(d) shows the SEM images of the active material of electrodes. AC powders of different particle size, graphite powders and PVDF formed a uniform electrode surface. Pores of different sizes form the active material surface which makes the brine water flow move freely in the active material.

3.2. Comparison of desalination performance of AC CDI electrodes with different current collectors

Fig. 3 shows the electrosorption/desorption and desalination performance of CDI electrodes with N-Al-CDI, M-Al-CDI, and Ni-CDI as the current collector. After electrosorption at 1.4 V for various lengths of time, the electrodes were mutually connected to be short-circuited to desorb the ions. The adsorbed ions released from the electrode surfaces returned to the solution leading to an increase in the conductivity of the NaCl solution [11,37]. After the desorption process, it is suggested that these electrodes have a good electrosorption/desorption performance.

The calculated salt adsorption capacity according to Eq. (2) represents desalination capacity. Clearly, M-Al-CDI electrode claims the highest desalination capacity at 1.4 V applied voltage, reaching 10.74 mg/g in 400 $\mu\text{s}/\text{cm}$ of NaCl solution, followed by Ni-CDI and N-Al-CDI electrodes. The lowest desalination capacity is found with N-Al-CDI electrode in 100 $\mu\text{s}/\text{cm}$ of NaCl solution which is 1.06 mg/g. The desalination capacity that enhanced with the water conductivities has increased from 100 to 400 $\mu\text{s}/\text{cm}$ because of the increase in solution conductivity, which can reduce the intrinsic resistance and enlarge the capacitor of CDI cell during the desalination process. M-Al-CDI boasts desalination efficiency up to 71% in 100 $\mu\text{s}/\text{cm}$ of solution and 53.2% in 400 $\mu\text{s}/\text{cm}$ of solution; Ni-CDI and N-Al-CDI show the same tendency. Although the desalination efficiency was higher in solution of lower concentration, the desalination capacity is higher in solution of higher concentration. This is because of the higher relative permittivity in higher concentration solution, which can enhance the EDLCs of electrodes.

The saturated electrosorption and desorption periods of M-Al-CDI electrode are the longest, around 50 and 30 min, respectively, and those of N-Al-CDI electrode are the shortest, 28 and 20 min, respectively.

3.3. Comparison of electrochemical behaviors of AC CDI electrodes

Fig. 4 shows the EIS Nyquist plots (at a bias voltage of 0 V) at the same scale (1 cm^2) of the N-Al-CDI, M-Al-CDI, and Ni-CDI electrodes. The frequency range is from 0.01 to 10,000 Hz, and the electrolyte is 1.0 M of KCl solution. The impedance spectra are composed of one semicircle at high frequency followed by a linear component at low frequency. At high frequencies, the intercept at real part (Z') is a combinational resistance of ionic resistance of the brine water, intrinsic resistance of the current collector, and interfacial resistance at the active material/current collector interface

(R_i) [38,39]. The same brine water was used as the electrolyte in the electrochemical test, so the resistance of the electrolyte was the same, R_i can be represented as the value of intrinsic resistance of the current collector and interfacial resistance.

At very high frequency, the electrode behaves like a pure resistance. In the middle frequency domain, the influence of the electrode porosity can be seen. At low frequency, the imaginary part sharply increases and a vertical line is observed, traducing a pure capacitive behavior. Clearly, the R_i of N-Al-CDI electrode is 57.2 Ω , that of Ni-CDI electrode is 26.4 Ω , and M-Al-CDI electrode is 5.1 Ω , which can be obtained from the intercept of the plots on real axis. The resistance of N-Al-CDI electrode is much higher than that of active material/M-Al. It is clear that the active material/N-Al surface contact is not optimum, due to a lack of adhesion of the active layer onto the native Al surface. On the other hand, the native alumina oxide layer present onto the Al surface hinders the electronic transfer between the Al collector and the active material. After alkali and electrochemical etching, the native oxide layer is removed and so are the barriers between the active material and the current collector. Furthermore, the resistance of M-Al-CDI electrode is lower because the surface contact between the M-Al current collector and the active material is increased, the electronic contact is improved, and more electrons are transferred from DC power to the surface of electrode, thus having enhanced the EDLCs. The electrode resistance of the active material/Ni is higher than that of the active material/M-Al because the electrical conductivity of Ni is less than that of Al, which leads to a higher intrinsic resistance in Ni-CDI.

Fig. 5 shows the CV curves at the same scale (1 cm^2) of the N-Al-CDI, M-Al-CDI, and Ni-CDI electrodes at the scanning rate of 5 mV/s. The electrolyte is 0.5 M of NaCl solution. Symmetric curves with respect to the X-axis are observed in M-Al-CDI, indicating that the capacitive process is a highly reversible and reliable process. The quasi-rectangular shapes point to the excellent EDLCs behavior. The CV curves of Ni-CDI and N-Al-CDI electrodes deviate from the rectangular shape, and the EDLCs behavior of the two electrodes is inferior to that of M-Al-CDI. The capacitances of M-Al-CDI are much higher than those of Ni-CDI and N-Al-CDI. Higher capacitance suggests that more ions in the salt water will reach the pores of the electrodes because of the lower intrinsic resistance, higher electric field intensity, and force on the electrodes.

Fig. 6 shows the charge/discharge performance of N-Al-CDI, M-Al-CDI, and Ni-CDI electrodes under 2 mL/min flow rate at a constant current density of 2 mA/ cm^2 and limit voltage of $V_{\text{max}} = 1.4$ V. The sampling interval is 5 s. The EDLCs are supposed to be charged from 0 to 1.4 V and discharged from 1.4 to 0 V. However, it is clear that the starting charge and discharge potentials slightly deviate (dV), and the potential loss of N-Al-CDI is larger than that of Ni-CDI and M-Al-CDI because internal resistance arises from resistances of the active materials and the current collector. The interfacial resistances between the electrolyte and the electrode and those between the current collector and the active material can be the contributor to create this internal resistance [6,40]. It is clear that the specific capacitance obtained in this research is in good agreement with desalination performance, EIS and CV studies.

The charge and discharge time of M-Al-CDI are the longest, because the slope of potential dV/dt is smaller than Ni-CDI and N-Al-CDI. The potential loss of M-Al-CDI is the smallest

during the charge and discharge process. These match what is presented in Fig. 3. The electroadsorption and desorption time of M-Al-CDI is longer than that of Ni-CDI and N-Al-CDI.

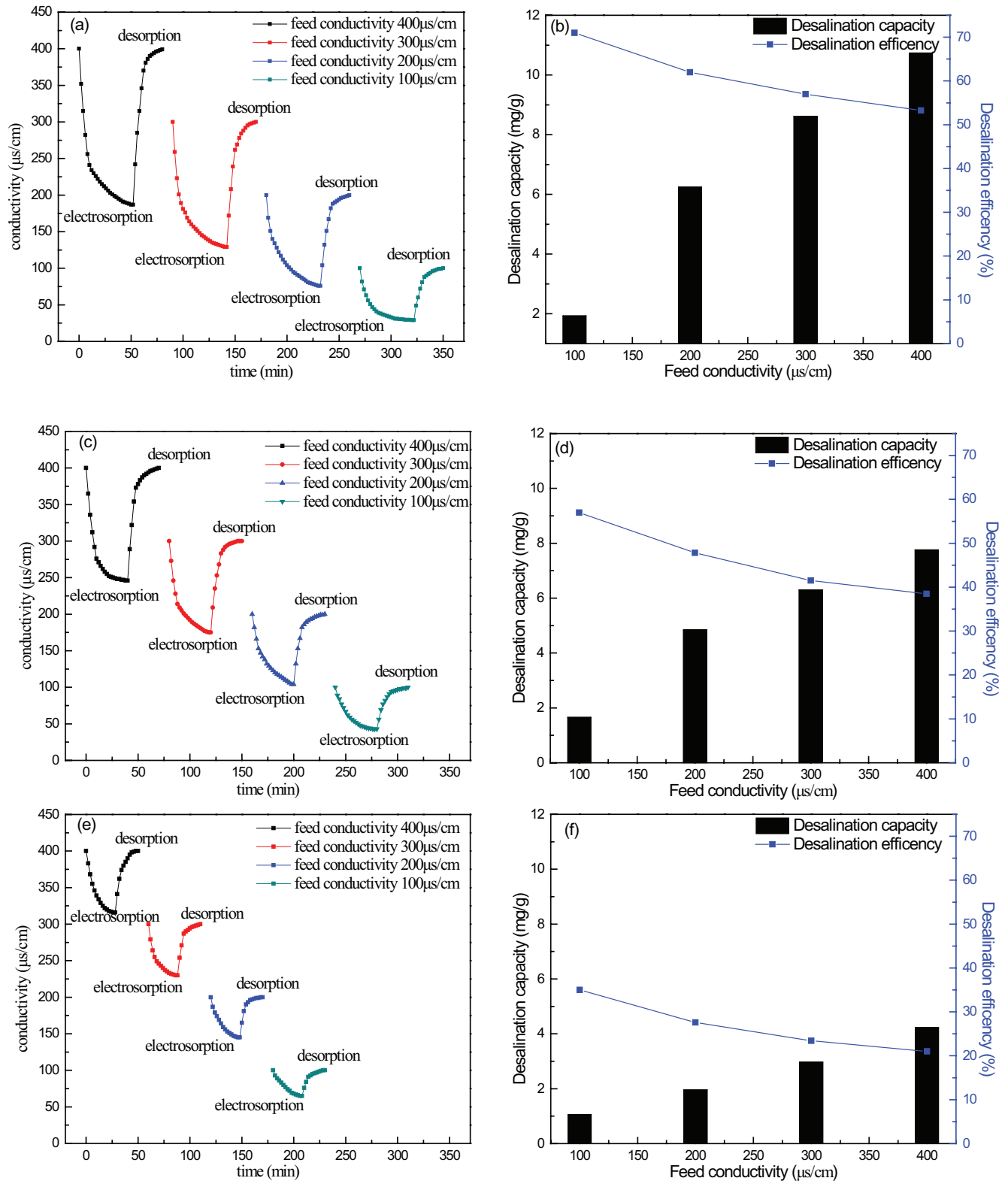


Fig. 3. Effect of feed conductivity on the desalination capacity and efficiency of the CDI process at 1.4 V applied voltage with (a, b) modified Al plate, (c, d) Ni foil, and (e, f) native Al plate as the current collector for CDI electrodes.

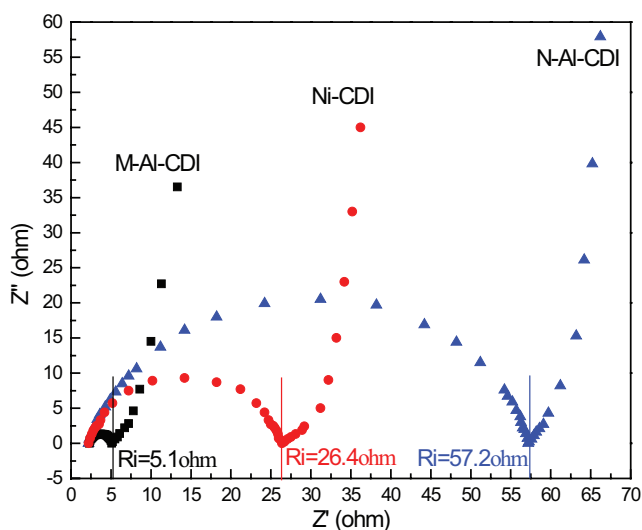


Fig. 4. EIS Nyquist plots at the same scale (1 cm^2) of the three different CDI electrodes with native Al plate (N-Al-CDI); modified Al Plate (M-Al-CDI), and Ni foil (Ni-CDI) as the current collector.

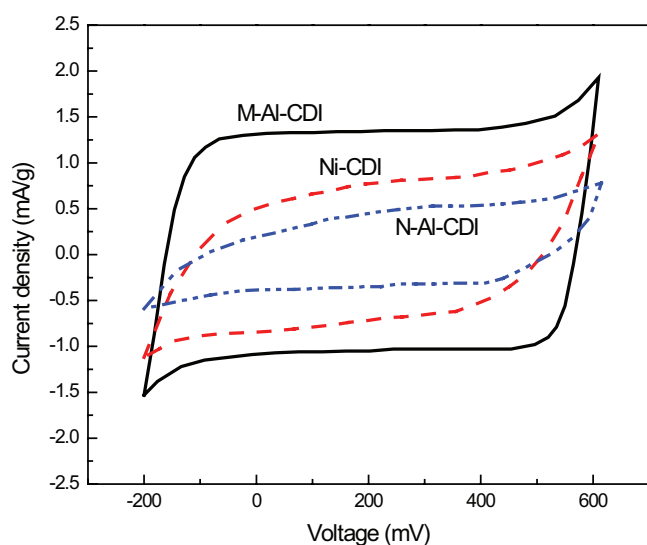


Fig. 5. CV curves of N-Al-CDI, M-Al-CDI, and Ni-CDI electrodes at the scanning rate of 5 mV/s in 0.5 M of NaCl solution.

4. Conclusions

CDI desalination ability and EDLCs can be greatly enhanced through the alkali and electrochemical etching of pure Al plate as the current collector in CDI electrode. The mechanisms might be attributed to that the alkali and electrochemical etching process increases the contact surfaces of the active material/Al current collector interface, enhances the electronic contact behavior, and reduces the intrinsic resistance, allowing more electrons to pass during the CDI process, which can increase the desalination capacitance and enlarge the EDLCs. The electrical conductivity of current collector has great impact on the capacitance of CDI process.

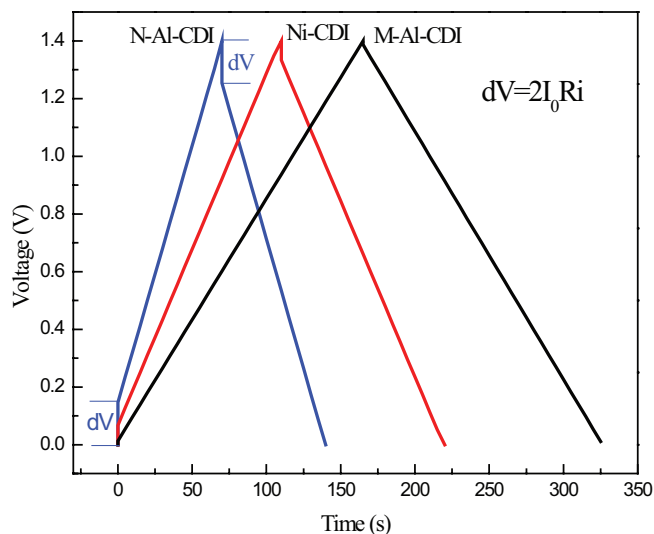


Fig. 6. Charge/discharge performance of different electrodes with different current collector.

Acknowledgment

This work was supported by National Science and Technology Support Programs of China (No. 2015BAB18B01) and key laboratory projects of Hubei province (No. 2016CFA086).

References

- [1] Y. Oren, Capacitive deionization (CDI) for desalination and water treatment—past, present and future (a review), *Desalination*, 228 (2008) 10–29.
- [2] Y. Chen, M. Yue, Z.H. Huang, Electrospun carbon nanofiber networks from phenolic resin for capacitive deionization, *Chem. Eng. Mater.*, 252 (2014) 8–15.
- [3] H.B. Li, L. Zou, Ion-exchange membrane capacitive deionization: a new strategy for brackish water desalination, *Desalination*, 275 (2014) 62–66.
- [4] P.M. Biesheuvel, R. Zhao, S. Porada, A. van der Wal, Theory of membrane capacitive deionization including the effect of the electrode pore space, *J. Colloid Interface Sci.*, 360 (2011) 239–248.
- [5] M.A. Anderson, A.L. Cudero, J. Palma, Capacitive deionization as an electrochemical means of saving energy and delivering clean water. Comparison to present desalination practices: will it compete? *Electrochim. Acta*, 55 (2010) 3845–3856.
- [6] A. Emmatifar, J.W. Palko, M. Stadermann, J.G. Santiago, Energy breakdown in capacitive deionization, *Water Res.*, 104 (2016) 303–311.
- [7] S.M. Jung, J.H. Choi, J.H. Kim, Application of capacitive deionization (CDI) technology to insulin purification process, *Sep. Purif. Technol.*, 98 (2012) 31–35.
- [8] S. Porada, R. Zhao, A. van der Wal, V. Presser, P.M. Biesheuvel, Review on the science and technology of water desalination by capacitive deionization, *Prog. Mater. Sci.*, 58 (2013) 1388–1442.
- [9] I. Cohen, E. Avraham, Y. Bouhadana, A. Soffer, D. Aurbach, Long term stability of capacitive de-ionization processes for water desalination: the challenge of positive electrodes corrosion, *Electrochim. Acta*, 106 (2013) 91–100.
- [10] G. Wang, C. Pan, L.P. Wang, Q. Dong, C. Yu, Z.B. Zhao, J.S. Qiu, Activated carbon nanofiber webs made by electrospinning for capacitive deionization, *Electrochim. Acta*, 69 (2012) 65–70.
- [11] W. Huang, Y.M. Zhang, S.X. Bao, R. Cruzb, S.X. Song, Desalination by capacitive deionization process using nitric acid-modified activated carbon as the electrodes, *Desalination*, 340 (2014) 67–72.

- [12] K.H. Park, D.H. Kwak, Electrosorption and electrochemical properties of activated-carbon sheet electrode for capacitive deionization, *J. Electroanal. Chem.*, 732 (2014) 66–73.
- [13] G. Wang, B.Q. Qian, Q. Dong, J.Y. Yang, Z.B. Zhao, J.S. Qiu, Highly mesoporous activated carbon electrode for capacitive deionization, *Sep. Purif. Technol.*, 103 (2013) 216–221.
- [14] M. Haro, G. Rasines, C. Macias, C.O. Ania, Stability of a carbon gel electrode when used for the electro-assisted removal of ions from brackish water, *Carbon*, 49 (2011) 3723–3730.
- [15] L. Zou, L.X. Li, H.H. Song, G. Morris, Using mesoporous carbon electrodes for brackish water desalination, *Water Res.*, 42 (2008) 2340–2348.
- [16] H. Oda, Y. Nakagawa, Removal of ionic substances from dilute solution using activated carbon electrodes, *Carbon*, 41 (2003) 1037–1047.
- [17] K. Sharma, R.T. Mayes, J.O. Kiggans, Jr., S. Yiacoumi, J. Gabitto, D.W. DePaoli, S. Dai, C. Tsouris, Influence of temperature on the electrosorption of ions from aqueous solutions using mesoporous carbon materials, *Sep. Purif. Technol.*, 116 (2013) 206–213.
- [18] R. Zhao, S. Porada, P.M. Biesheuvel, A. van der Wal, Energy consumption in membrane capacitive deionization for different water recoveries and flow rates, and comparison with reverse osmosis, *Desalination*, 330 (2013) 35–41.
- [19] O.N. Demirel, R.M. Naylor, C.A.R. Perez, E. Wilkes, C. Hidrovo, Energetic performance optimization of a capacitive deionization system operating with transient cycles and brackish water, *Desalination*, 314 (2013) 130–138.
- [20] X. Gao, A. Omosibi, J. Landon, K.L. Liu, Enhancement of charge efficiency for a capacitive deionization cell using carbon xerogel with modified potential of zero charge, *Electrochem. Commun.*, 39 (2014) 22–25.
- [21] C.C. Huang, J.C. He, Electrosorptive removal of copper ions from wastewater by using ordered mesoporous carbon electrodes, *Chem. Eng. J.*, 221 (2013) 469–475.
- [22] J.J. Lado, R.E. Pérez-Roa, J.J. Wouters, M.I. Tejedor-Tejedor, M.A. Anderson, Evaluation of operational parameters for a capacitive deionization reactor employing asymmetric electrodes, *Sep. Purif. Technol.*, 133 (2014) 236–245.
- [23] M.W. Ryoo, G. Seo, Improvement in capacitive deionization function of activated carbon cloth by titania modification, *Water Res.*, 37 (2003) 1527–1534.
- [24] L. Zou, G. Morris, D. Qi, Using activated carbon electrode in electrosorptive deionization of brackish water, *Desalination*, 225 (2008) 329–340.
- [25] L.K. Pan, X.Z. Wang, Y. Gao, Y.P. Zhang, Y.W. Chen, Z. Sun, Electrosorption of anions with carbon nanotube and nanofibre composite film electrodes, *Desalination*, 244 (2009) 139–143.
- [26] L.C. Han, K.G. Karthikeyan, M.A. Anderson, J.J. Wouters, K.B. Gregory, Mechanistic insights into the use of oxide nanoparticles coated asymmetric electrodes for capacitive deionization, *Electrochim. Acta*, 90 (2013) 573–581.
- [27] M.T.Z. Myint, J. Dutta, Fabrication of zinc oxide nanorods modified activated carbon cloth electrode for desalination of brackish water using capacitive deionization approach, *Desalination*, 305 (2012) 24–30.
- [28] M.E. Suss, T.F. Bauman, M.A. Worsley, K.A. Rose, T.F. Jaramillo, M. Stadermann, J.G. Santiago, Impedance-based study of capacitive porous carbon electrodes with hierarchical and bimodal porosity, *J. Power Sources*, 241 (2013) 266–273.
- [29] H. Ab, M. Kubota, M. Nemoto, Y. Masuda, Y. Tanaka, H. Munakata, K. Kanamura, High-capacity thick cathode with a porous aluminum current collector for lithium secondary batteries, *J. Power Sources*, 334 (2016) 78–85.
- [30] E. Cho, J.Y. Mun, O.B. Chae, O.M. Kwon, H.T. Kim, J.H. Ryu, Y.G. Kim, S.M. Oh, Corrosion/passivation of aluminum current collector in bis(fluorosulfonyl) imide-based ionic liquid for lithium-ion batteries, *Electrochem. Commun.*, 22 (2012) 1–3.
- [31] B. Bhujun, M.T.T. Tan, A.S. Shanmugam, Evaluation of aluminium doped spinel ferrite electrodes for supercapacitors, *Ceramics Int.*, 42 (2016) 6457–6466.
- [32] M. Li, F. Liu, J.P. Cheng, J. Ying, X.B. Zhang, Enhanced performance of nickel–aluminum layered double hydroxide nanosheets/carbon nanotubes composite for supercapacitor and asymmetric capacitor, *J. Alloys Compd.*, 635 (2015) 225–232.
- [33] S.W. Woo, S.T. Myung, H. Bang, D.W. Kim, Y.K. Sun, Improvement of electrochemical and thermal properties of $\text{Li}[\text{Ni}_{0.8}\text{Co}_{0.1}\text{Mn}_{0.1}]\text{O}_2$ positive electrode materials by multiple metal (Al, Mg) substitution, *Electrochim. Acta*, 54 (2009) 3851–3856.
- [34] Y.I. Hsu, K. Masutani, T. Yamaoka, Y. Kimura, Strengthening of hydrogels made from enantiomeric block copolymers of polylactide (PLA) and PEG by the chain extending DielsAlder reaction at the hydrophilic PEG terminals, *Polymer*, 67 (2015) 157–166.
- [35] G.Z. Li, J.X. Li, W. Tan, H. Jin, H.X. Yang, J.H. Peng, C.J. Barrow, M. Yang, H.B. Wang, W.R. Yang, Preparation and characterization of the hydrogen storage activated carbon from coffee shell by microwave irradiation and KOH activation, *Int. Biodeterior. Biodegrad.*, 113 (2016) 386–390.
- [36] A.M. Dehkoda, E. Gyenge, N. Ellis, A novel method to tailor the porous structure of KOH-activated biochar and its application in capacitive deionization and energy storage, *Biomass Bioenergy*, 87 (2016) 107–121.
- [37] J. Gamby, P.L. Taberna, P. Simon, J.F. Fauvarque, M. Chesneau, Studies and characterisations of various activated carbons used for carbon/carbon supercapacitors, *J. Power Sources*, 101 (2001) 109–116.
- [38] X.X. Zhang, F. Ran, H.L. Fana, Y.T. Tan, L. Zhao, X.M. Lia, L.B. Kong, L. Kang, A dandelion-like carbon microsphere/ MnO_2 nanosheets composite for supercapacitors, *J. Energy Chem.*, 23 (2014) 82–90.
- [39] C.W. Liew, S. Ramesh, Studies on ionic liquid-based corn starch biopolymer electrolytes coupling with high ionic transport number, *Cellulose*, 20 (2013) 3227–3237.
- [40] H.B. Li, L.K. Pan, Y.P. Zhang, L. Zou, C.Q. Sun, Y.K. Zhan, Z. Sun, Kinetics and thermodynamics study for electrosorption of NaCl onto carbon nanotubes and carbon nanofibers electrodes, *Chem. Phys. Lett.*, 485 (2010) 161–166.